analytical chemistry

Article

pubs.acs.org/ac

A Microfluidic Platform for the Rapid Determination of Distribution Coefficients by Gravity-Assisted Droplet-Based Liquid−Liquid Extraction

Carl Esben Poulsen,[†] Robert C. R. Wootton,[‡] Anders Wolff,[†] Andrew J. deMello,[‡] and Katherine S. Elvira*[,‡]

[†]Department of Micro- and Nanotechnology, Technical University of Denmark, Kgs. Lyngby, Denmark

[‡]Institute of Chemical and Bioengineering, Department of Chemistry and Applied Biosciences, ETH Zurich, Zurich, Switzerland

Supporting Information

ABSTRACT: The determination of pharmacokinetic properties of drugs, such as the distribution coefficient (D) is a crucial measurement in pharmaceutical research. Surprisingly, the conventional (gold standard) technique used for D measurements, the shake-flask method, is antiquated and unsuitable for the testing of valuable and scarce drug candidates. Herein, we present a simple microfluidic platform for the determination of distribution coefficients using droplet-based liquid−liquid extraction. For simplicity, this platform makes use of gravity to enable phase separation for analysis and is 48 times faster and uses 99% less reagents than performing an equivalent measurement using the shake-flask method. Furthermore, the D measurements achieved in our platform are in good agreement with literature values measured using traditional shake-flask techniques. Since D is affected by volume ratios, we use the apparent acid dissociation constant, pK', as a proxy for intersystem comparison. Our platform determines a pK' value of 7.24 ± 0.15, compared to 7.25 ± 0.58 for the shake-flask method in our hands and 7.21 for the shake-flask method in the literature. Devices are fabricated using injection molding, the batchwise fabrication time is <2 min per device (at a cost of $1 U.S. per device), and the interdevice reproducibility is high.

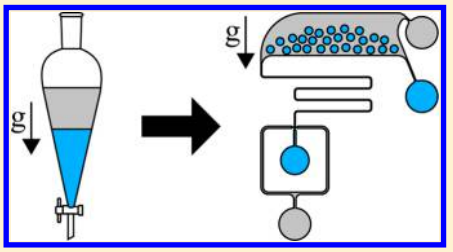

The pharmacokinetic properties of drugs are key indicators of how a drug will perform in the human body. The objective behind the study of these properties is to allow prediction of the viability of a drug prior to its administration to human subjects so that the cost and high attrition rates associated with drug discovery can be mitigated. One of the most commonly used metrics to determine pharmacokinetic properties is the distribution coefficient (D), which is an important indicator of the interaction between a compound and cellular membranes and, hence, allows the prediction of the extent of absorption of orally administered drugs.

The standard experimental methodology for measuring distribution coefficients is the shake-flask method, where the distribution of a drug between a hydrophilic (aqueous) phase and a hydrophobic phase (normally octanol) is measured through use of a separating funnel or centrifuge.[1] The advantages associated with this method are historical and based on the experimental simplicity and availability of the required equipment in normal laboratory settings. However, such measurements take a long time, since the phases must be pre-equilibrated with the opposite phase over the course of 24 h,[1] and large volumes are required, which is problematic when assaying valuable drug samples.[2] Furthermore, D is known to be sensitive to contaminants.[1]

The adoption of microfluidic technologies provides interesting alternatives to the shake-flask method. Microfluidic platforms specialize in the manipulation of fluids on the microscale, with key advantages related to reduced sample sizes, enhanced assay speed, and increased control over physical and chemical characteristics associated with the system under study.[3] However, microfluidic platforms have not become *de rigueur* for distribution coefficient measurements because of factors related to the material used for fabrication, phase control, and overall system complexity. For example, microfluidic platforms presented in the literature have been fabricated in materials that scale poorly or are too expensive for commercial-scale production, such as polydimethylsiloxane (PDMS),[4−7] glass,[8−10] silicon,[11,12] and polymers (such as thiolene,[13] SIFEL,[13] or NOA81[14]) or require surface modification[5] prior to use. Both these characteristics make commercial application of such platforms unfeasible. Furthermore, many microfluidic platforms have used the co-flow of oil and water phases through a device,[4,11,13] which requires complicated structures for phase separation and stabilization (such as the use of porous fluoropolymer membranes[2,11]), or relies on surface modification of wetting characteristics to stabilize the co-flowing phases.[5,8,13]

An alternative microfluidic method for liquid−liquid extraction makes use of droplets, which maximize the available surface area for the partitioning of compounds between the

Received: March 19, 2015
Accepted: May 18, 2015
Published: May 18, 2015

DOI: 10.1021/acs.analchem.5b01061
Anal. Chem. 2015, 87, 6265−6270

immiscible phases. These systems have the advantage of allowing easy removal of artifacts, since each droplet defines a single measurement and, hence, contaminants are easily identified. Droplet-based microfluidic systems are in fact closely related to the shake-flask method, where phase agitation causes emulsification prior to phase separation by allowing the mixture to re-equilibrate using gravity. However, microfluidic droplet-based systems normally use surfactants to stabilize droplets[15] and, hence, require complicated techniques to drive de-emulsification for phase separation, such as the use of strong electric fields,[12] or require complicated detection methods to perform in-droplet measurements, such as laser-induced fluorescence.[9]

It is clear that microfluidic platforms have the potential to revolutionize the measurement of distribution coefficients, especially for high-value drugs, and to ensure that these measurements are user-independent and considerably faster than conventional methods. However, for microfluidic platforms to achieve this goal, they must be easy to use, inexpensive to produce commercially, of simple design, disposable, and able to provide a clear advantage over the shake-flask technique. The use of microfluidic technologies in commercial applications is an enduring goal in the field, but very few microfluidic platforms are commercially viable, specifically because of factors such as the material used for fabrication and ease of use. Herein, we present a droplet-based microfluidic platform for the determination of distribution coefficients using gravity to separate the phases for analysis. The platform is fabricated using injection molding and can be easily integrated into a production line. The devices are low-cost and, hence, disposable, which we demonstrate through the analysis of data gathered using over 30 devices. The material used for device fabrication is compatible with the solvent systems used for distribution coefficient measurements, and we show that our microfluidic platform performs in a superior manner to the shake-flask method, specifically where cost, reagent volume, and experimental time are paramount.

MATERIALS AND METHODS

Design of the Microfluidic Platform. The microfluidic platform was designed to maximize the interaction between the aqueous and oil phases and ensures optimal mass transfer through the use of aqueous-in-oil droplets. After creation at a flow focusing geometry, droplets enter the separation chamber (Figure 1, Video S1 in the Supporting Information (SI)). Extended droplet residence times in this chamber allow the droplets to travel a significant portion of the chamber width (w) relative to the continuous phase due to gravity (further details of these calculations can be found in section S1 in the Supporting Information), hence allowing the removal of aqueous droplets from the continuous oil phase for further analysis of the oil phase. In other words, gravitational forces allow aqueous droplets to settle at the bottom of the separation chamber and hence exit at the lower, aqueous, outlet. This allows the droplet-free oil phase to be collected from the upper outlet and used for absorption measurements.

As described in detail in section S1 in the Supporting Information, if gravity is to enable an aqueous droplet suspended in octanol to migrate at least the entire width of the separation chamber, relative to the continuous phase, the following inequality must be fulfilled:

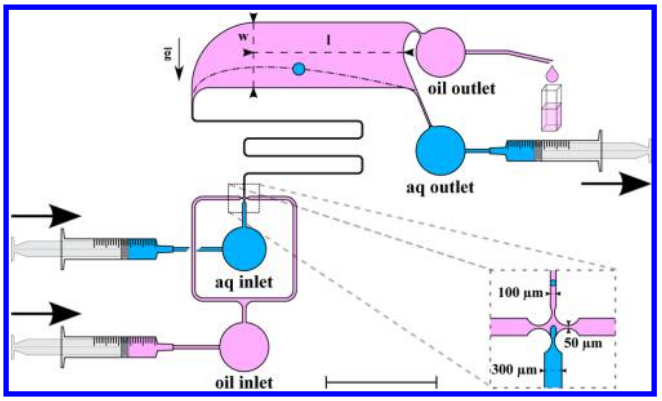

Figure 1. Scale drawing of the microfluidic platform used for droplet-based liquid−liquid extraction (the syringes and the cuvette at the oil outlet are not to scale). Droplets are formed at a flow focusing geometry and then inserted into a large separation chamber where gravity ($\vec{g}$) enables separation of the two phases. Blue denotes the aqueous (aq) phase, and pink denotes the oil phase. The width (w) of the separation chamber is 6 mm, its length (l) is 13.7 mm, and the channel height is 100 μm throughout. The width of the channels connecting both outlets to the separation chamber is 150 μm. The oil phase was collected in a cuvette at the oil outlet, and absorbance measurements were performed as detailed in the liquid−liquid extraction section. The scale bar in the main figure is 10 mm, and the enlarged area shows the dimensions of the flow focusing geometry used for droplet generation. Single-headed arrows denote the directions of flow from the syringe pumps and of gravity. The images of syringes and the cuvette are taken from Wikimedia.org and are used under a creative commons license.

$$\frac{\tilde{d}^2\tilde{h}\tilde{l}}{\tilde{Q}_{tot}} \geq 18N_{St} \quad (1)$$

where $\tilde{d}$ is the dimensionless droplet diameter, $\tilde{h}$ the dimensionless height of the separation chamber, $\tilde{l}$ the dimensionless chamber length, $\tilde{Q}_{tot}$ the dimensionless total flow rate, and N_{St} the Stokes number (the ratio of viscous to gravitational forces). Therefore, in the microfluidic platform used herein, where h = 100 μm, w = 6 mm, l = 13.7 mm, and $d \leq h$, the total flow rate should be kept smaller than 20.8 μL/min. It is important to note that this value defines the maximum flow rate, since smaller droplets will have a lower terminal velocity and will hence require a longer residence time in the separation chamber to allow for a channel width migration. Furthermore, the Bond number (Bo) is $\leq$ 0.0031, confirming that surface tension forces dominate in our platform and, hence, droplets are round (for details of the interfacial tension measurements used to determine the Bo, see section S3 in the SI).

Chip Fabrication. *Micromilling.* A structured mold insert for injection molding was designed in Autodesk Inventor Professional 2012, converted to G-code in CimatronE10, and fabricated in 2017 aluminum alloy (MetalCentret, Denmark) by micromilling (NTI CADcenter A/S, Denmark). Energy directors for ultrasonic welding[16] were defined using a 60° helical engraving tool (No. 7025, DIXI polytool, Herstad +Piper, Denmark) producing 50-μm-high prism-shaped energy directors.

Injection Molding. The aluminum mold insert and a matching countermold with 12 ISO Luer-fittings[17] were installed in a Victory 80/45 Tech injection molder (Engel, Austria). The polymer used for injection molding was COC

DOI: 10.1021/acs.analchem.5b01061
Anal. Chem. 2015, 87, 6265−6270

(Grade 5013L-10, TOPAS Advanced Polymers, Germany) with a glass transition temperature (T_g) of 135 °C. The injection temperature of the polymer was 270 °C, and the mold and demolding temperatures were kept stable at 120 °C.

Ultrasonic Welding. To seal the microfluidic device, a 152 μm thick COC sheet (Grade 5013S-04, TOPAS Advanced Polymers, Germany) was bonded to the injection molded piece using a Telsonic-USP4700 ultrasonic welder (Telsonic, Herstad +Piper, Denmark). The welding was conducted using 45 J at 90% amplitude and 20 kHz, with a trigger force on the piece of 600 N in the normal direction.

Annealing. To avoid solvent-induced cracking, internal stress from the isothermal injection molding and ultrasonic welding was removed by annealing. The entire batch of chips (200 pieces) was loaded into an oven, which was cycled from room temperature to 125 °C and back to room temperature over a period of 2 h. A comparison of solvent-induced stress cracking in annealed and nonannealed chips due to octanol exposure is shown in section S5 in the SI.

Overall, including handling, the total turn-around time per chip was 40 s for injection molding, 20 s for ultrasonic welding, and 36 s for annealing, which amounts to a fabrication time of less than 2 min per device.

Liquid–Liquid Extraction. Standards for determining quinine extinction coefficients were prepared by dissolving quinine hydrochloride dihydrate (≥99.0%, Sigma-Aldrich, Switzerland) either in 1× DPBS (Dulbecco's phosphate-buffered saline, pH 7.4, Life Technologies, Switzerland) or in octan-1-ol (≥99.0%, Alfa Aesar, Germany) with 3% (w/w) ABIL EM90 (cetyl dimethicone copolyol, Rose Chemicals, U.K.). The DPBS and octanol used in the preparation of the standards were stored with 5% octanol and DPBS, respectively, to ensure mutual saturation of the two phases.

Samples for "bulk" analyses were prepared in glass vials with aqueous to octanol (aqueous/octanol) volume ratios of 2:1, 1:1, 1:2, 1:4, 1:8, 1:16, 1:32, and 1:10, the latter of which creates a bulk sample with a volume ratio similar to the flow rate ratio in the droplet-based experiments. The total volume for each sample was 4 mL, and all eight concentrations were prepared in triplicate, for a total of 24 samples. All aqueous and octanol volumes were calculated from mass measurements and density to ensure consistency. At the start of each experiment, the aqueous solution contained 1 mM quinine hydrochloride dihydrate.

Droplet-based liquid–liquid extraction was conducted on the microfluidic platform described above using three Aladdin syringe pumps (AL-1000, WPI-Europe, U.K.) mounted with 500 μL Hamilton gas-tight syringes (VWR, Denmark): two for controlling the inlet flow rates and one for controlling the aqueous outlet flow rate. Assuming the system is operated under a stable flow for 30–90 min per experiment, the oil outlet flow rate was assumed to satisfy the continuity equation

$$0 = Q_{aq,in} + Q_{oil,in} + Q_{aq,out} + Q_{oil,out}$$

where the subscripts "aq" and "oil" denote aqueous and oil phases, respectively, and the subscripts "in" and "out" denote the direction of flow as into and out of the microfluidic device, respectively. The aqueous outlet flow rate ($Q_{aq,out}$) was set to 3.5 μL/min, and this ensures that no droplets exit from the oil outlet, that the flow at the oil outlet is stable, and that enough oil can be collected to finish the experiment within 30 min. During the experiment, the microfluidic device was mounted such that the width of the separation chamber was parallel to the gravitational force (see $\vec{g}$ in Figure 1). The absorbance of the oil phase was measured by collecting a set volume of oil from the oil outlet and performing off-line measurements at 340 nm on a BioPhotometer Plus system (Eppendorf, Switzerland) using UVette cuvettes (Eppendorf, Switzerland). For the measurement of absorbance values in the range of 0.05 to 1.00, both the 10 mm and the 2 mm path lengths of the cuvettes were used. Quinine concentrations determined from absorbance measurements using the Beer–Lambert law were used to calculate D (see the SI for further information). The parameters used for on-chip liquid–liquid extraction are summarized in Table 1.

Table 1. Parameters for On-Chip Liquid–Liquid Extraction[a]

	(+)	(x)
$Q_{aq,in}$ (μL/min)	0.5	1.0
$Q_{oil,in}$ (μL/min)	5.0	5.0
$Q_{aq,out}$ (μL/min)	3.5	3.5
$r_Q = Q_{oil,in}/Q_{aq,in}$	10	5
Quinine concentration (μM)	100, 250, 500, 750, 1000	
Number of experiments	3	3
Total number of devices	15	15

[a]The red plus sign symbol (+) and the blue cross symbol (×) denote datasets of unique r_Q and will be used for identification in Figures 3 and 4.

On-chip droplet imaging was performed using a Manta G046B ASG camera (Allied Vision, Denmark) mounted on a (1–4)× adjustable zoom lens. Images were subsequently analyzed using a custom-made MATLAB algorithm incorporating circle detection by circular Hough transform to determine droplet size.

RESULTS AND DISCUSSION

Characterization of the Microfluidic Platform. The performance of the microfluidic platform over a range of aqueous and oil flow rates is illustrated in Figure 2, in terms of droplet size statistics. During initial device characterization, it

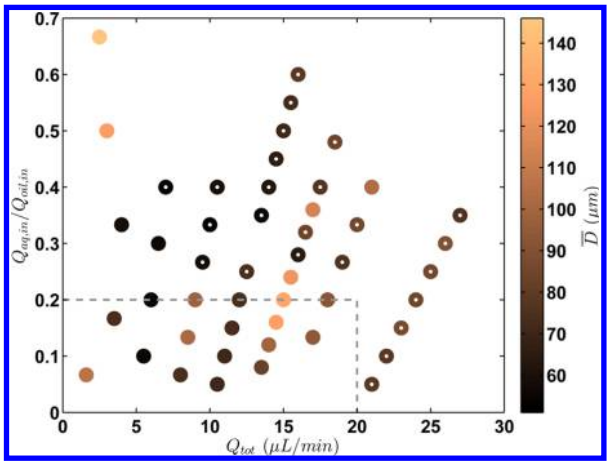

Figure 2. Characterization of droplet formation on the microfluidic device. Average droplet diameter (color map) versus total flow rate (Q_{tot}) and versus the flow rate ratio ($Q_{aq,in}/Q_{oil,in}$). Data points with a white dot represent system conditions where the droplet residence time is too low to allow phase separation, calculated using eq S2 in the SI. The section highlighted by the dashed rectangle denotes the parameter space where flow rate combinations allow efficient droplet guidance. Note that the separation chamber has a height of 100 μm, and, hence, droplets with a larger diameter are nonspherical.

DOI: 10.1021/acs.analchem.5b01061
Anal. Chem. 2015, 87, 6265–6270

was found that configurations of $Q_{aq,in}/Q_{oil,in} > 0.2$ produced too many droplets for efficient droplet migration and hence separation of the phases at the device outlets. Since droplets at these flow rates do not leave the chamber quickly enough, the high droplet density effectively constricts the chamber dimensions, causing new droplets to have higher flow rates and thus lower residence times. This phenomenon is related to hydraulic damming and, practically, means that droplets agglomerate at the aqueous outlet, causing new droplets to exit via the oil outlet. The box in Figure 2 highlights the maximum flow rate ($Q_{tot} = Q_{aq,in} + Q_{oil,in} = 20$ μL/min) and inlet flow rate ratio ($Q_{aq,in}/Q_{oil,in} = 0.2$) at which droplets can be separated from the oil flow at the maximum droplet diameter ($d = h$). This is the region in which $\tilde{s}_w \leq \tilde{w}$ and the boundaries of the box depend on the droplet size because smaller droplets have a lower terminal velocity (further details can be found in section S1 in the SI). Figure 2 clearly shows the robustness of the microfluidic platform in terms of the variety of flow rate combinations at which stable droplet production is possible.

The interdevice droplet production reproducibility was measured in triplicate under the experimental conditions described in Table 1. The statistical analysis of these data is summarized in Table 2. It is evident that the produced droplets

Table 2. Droplet Size Statistics for On-Chip Liquid−Liquid Extraction Experiments[a]

$Q_{aq,in}$ (μL/min)	$Q_{oil,in}$ (μL/min)	$\overline{CV_D}$[b] (%)	$\bar{\bar{d}}$[c] (μm)	$SEM_{\bar{d}}$[d] (μm)
1.0	5.0	34.1 ± 9.3	70.9	19.7
0.5	5.0	33.7 ± 6.8	66.2	9.55

[a]The statistical analysis is based on droplet images acquired in the experiments described in Table 1, and each image contained a minimum of 50 droplets (on average, there were 384 droplets per image). Each set of flow rate conditions was analyzed in 15 individual experiments on 15 different microfluidic platforms. [b]$\overline{CV_D}$ is the average coecient of variation of droplet diameters. [c]$\bar{\bar{d}}$ is the grand mean of droplet diameters is defined as the arithmetic mean of the arithmetic mean. [d]$SEM_{\bar{d}}$ is the standard error of the arithmetic mean of droplet diameters.

have a high polydispersity ($\overline{CV_D} \approx 34\% \pm 8.1\%$) but that average droplet diameters are conserved across different microfluidic devices ($SEM_{\bar{d}} \approx 15$ μm). As shown in Figure 1, the flow-focusing geometry used for droplet creation has rounded edges, which explains the high polydispersity when compared to other microfluidic platforms where the droplet formation geometry has sharp corners. These rounded edges are caused by a limitation of the milling process which, unlike lithographic methods, defines geometries by material removal using milling tools of finite diameters (200 μm). In addition, micromilling introduces surface roughness, which may also introduce variations during droplet breakoff and formation.

Liquid−Liquid Extraction. To verify that on-chip liquid−liquid extraction was not limited by diffusion at low droplet residence times, extractions were conducted with aqueous quinine concentrations of 100 μM, 250 μM, 500 μM, 750 μM, and 1 mM, at aqueous flow rates of 1 μL/min and 0.5 μL/min and with a constant oil flow rate of 5 μL/min throughout. The distribution of quinine between the aqueous and oil phases is described by the relationship between the inbound aqueous mass flow rate ($I_{aq,in}$) and the outbound oil mass flow rate ($I_{oil,out}$), as shown in Figure 3, where $I = cQ$ and c is the

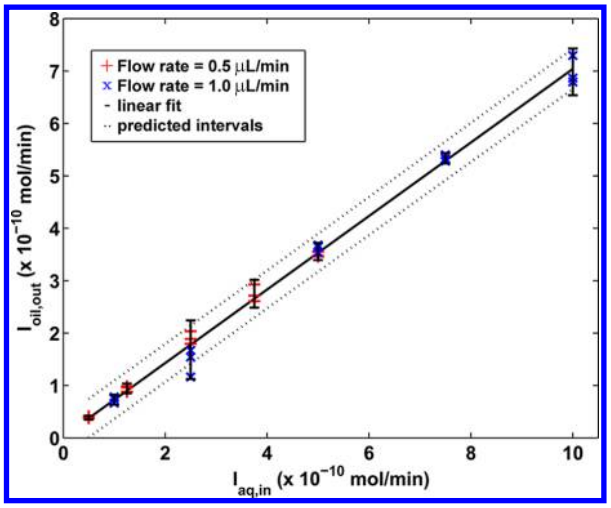

Figure 3. Outbound versus inbound molar flow rates for on-chip liquid−liquid extraction. The inbound molar flow rate is varied by adjusting the aqueous flow rate and hence the aqueous quinine concentration. The concentration of quinine was calculated using extinction coefficient data shown in Figure S3 in the SI. Error bars show two standard deviations from the mean. Prediction intervals were calculated using the MATLAB package *polyconf* and illustrate the upper and lower bounds in which 95% of future data points will fall.

concentration. Since the outbound mass flow rate is observed to scale linearly with the inbound mass flow rate, the system is at equilibrium when the phases are separated for analysis. If the residence time of the droplets in the separation chamber was insufficient to allow for mass transfer equilibrium, variations in the inbound mass flow rate introduced by varying the flow rate (and hence the residence time of the droplets) or the aqueous quinine concentration would result in a nonlinear relationship between $I_{oil,out}$ and $I_{aq,in}$. The two total flow rates used in this study of 5.5 and 6.0 μL/min cause average residence times of 129 and 118 s, respectively. The fastest droplets shown in Video S1 in the SI have a residence time of 68 s. Our average residence times are at least 1 order of magnitude more than what was needed to achieve a steady state in diffusion studies of fluorophores in larger droplets (equilibrium was reached in less than 8 s).[7,18]

In order to assess the performance of liquid−liquid extraction on the droplet microfluidic platform compared to standard methodologies, the distribution coefficients of quinine from bulk overnight experiments and on-chip liquid−liquid extractions are compared in Figure 4. For bulk experiments, this figure shows the distribution coefficients determined at the volume ratios stated in the Materials and Methods section. Equation 2 was used to calculate the apparent acid dissociation constant, pK',[19] which is unique to the system (pH and buffer) and, unlike the distribution coefficient, is independent of the volume ratio.

$$D = \frac{V_{aq}}{V_{oil}}(10^{pK_a - pK' - 1}) \quad (2)$$

Here, V is volume and pK_a is the true acid dissociation constant. Table 3 summarizes the experimental values of pK' both from bulk and on-chip droplet based liquid−liquid extraction experiments, and from the literature. The pK_a value used to calculate pK' from eq 2 was 8.505, which defines the average of two literature values: 8.58[20] and 8.43.[21]

DOI: 10.1021/acs.analchem.5b01061
Anal. Chem. 2015, 87, 6265−6270

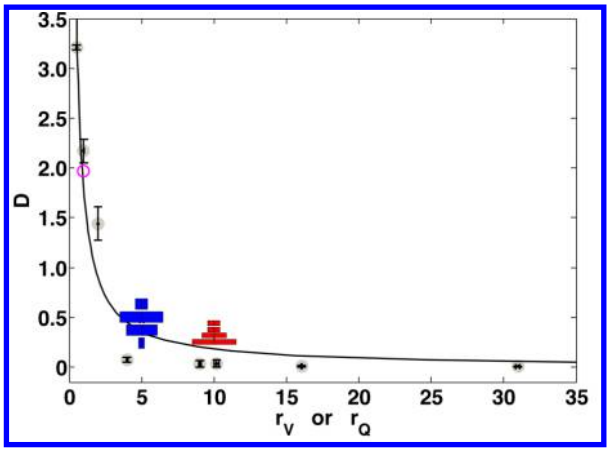

Figure 4. Distribution coefficients, D, both from bulk experiments (depicted by gray circles with black error bars representing the standard deviation) plotted versus volume ratio, $r_V = V_{oil}/V_{aq}$, and from on-chip liquid–liquid extraction experiments at aqueous flow rates of 0.5 μL/min (red violin plot) and 1.0 μL/min (blue violin plot) plotted versus the volume flow rate ratio, $r_Q = Q_{oil,in}/Q_{aq,in}$. The concentration of quinine was calculated using extinction coefficient data shown in Figure S3 in the SI. The distribution of data points from on-chip experiments are illustrated as violin plots to highlight the large amount of measurements gathered for each data point when using a microfluidic platform (each violin plot incorporates data gathered from 15 separate experiments as detailed in Table 1). The solid line represents the least squares fit of eq 2 for the data from bulk experiments, $D = (10^{pK_a - pK' - 1}) \times (1/r_V) = 10^{0.25} \times (1/r_V)$. The open pink circle represents literature data.[20]

As is evident from the data presented in Table 3, there is good agreement between the pK' values measured in bulk and on-chip experiments, and these values are also in good agreement with the literature. Table 4 shows how other parameters such as cost and reagent consumption compare between microfluidic and traditional methodologies. In terms of cost efficiency (reagent consumption and time) and sensitivity to user interference, the microfluidic platform greatly outperforms traditional methodologies. Furthermore, it is possible to perform continuous measurements using the microfluidic platform, such as in-line absorbance measurements, and during one continuous experiment in the microfluidic platform, the variation of combinations of $Q_{aq,in}$ and $Q_{oil,in}$ allows for the concurrent acquisition of multiparameter data (e.g., r_Q, D).

CONCLUSIONS

The microfluidic devices presented herein are fabricated using injection molding, ultrasonic welding, and annealing, which are all processes currently used in commercial manufacturing, with a time per device of <2 min. We demonstrate the reliability of the devices by performing experiments on 30 different devices, with distribution coefficient data gathered on these platforms showing close agreement with literature values and low statistical variation under a variety of flow conditions and concentrations. To enable the use of this platform in nonspecialist laboratory settings, the device design is simple, and gravity is used to enable phase separation. Finally, we assess the parameters associated with this microfluidic platform, in comparison to the shake-flask method. We show that our microfluidic platform is 48 times faster and uses 99% less reagents than the shake-flask method. In addition, user sensitivity and contamination, which are sources of error for conventional techniques, are negligible in our platform. As future work, the system will be integrated with online absorption detection to allow extraction of data from individual droplets to enhance analytical efficiency.

Table 4. Comparison of Parameters Associated with Bulk and On-Chip Methodologies for Liquid–Liquid Extraction

	bulk	on-chip
experiment time	>24 h	30 min
reagent volume	>20 mL	300 μL
cost of reagents	>25 US dollars	0.37 US dollars
cost of microfluidic device	N/A[a]	1 US dollars
sensitivity to user interference	high	low
repeatability	good	good
continuous measurements	not possible	possible
phase space sweep	not possible	possible

[a]N/A = not applicable.

ASSOCIATED CONTENT

Supporting Information

A mathematical description and a two-dimensional numerical (COMSOL) model of the effect gravity has on droplets in the separation chamber, experimental data to verify our model, absorbance data at different quinine concentrations and equations used to calculate the extinction coefficient of quinine, interfacial tension measurements of our octanol/DPBS/Abil EM90 system required to calculate the Bond number, derivations of the equations used for calculating D from quinine concentrations, and data to show the effect that annealing has on ultrasonically welded devices; a video of gravity-assisted droplet-based liquid–liquid extraction. The Supporting Information is available free of charge on the ACS Publications website at DOI: 10.1021/acs.analchem.5b01061.

AUTHOR INFORMATION

Corresponding Author

*E-mail: katherine.elvira@chem.ethz.ch.

Notes

The authors declare no competing financial interest.

Table 3. Comparison of Experimental Data Gathered from Bulk and Microfluidic Experiments with Literature Values[a]

	r_V or r_Q	D	pK'
Data from bulk experiments, (●)	1/2 to 32/1	Fig. 4	7.25 ± 0.58
Data from on-chip experiments, (+) and (x)	5.0/1.0 and 5.0/0.5	Fig. 4	7.24 ± 0.15
Data from literature,[20] (○)	1	1.97	7.21

[a]The apparent acid dissociation constant, pK', was calculated from volume or flow rate ratios, r_V or r_Q, using D at pH 7.4, a pK_a value of 8.505,[20,21] and eq 2. The markers (gray circle, red plus sign (+), blue cross symbol (×), and pink open circle (○) used in the table refer to Figure 4. Error estimations in the pK' values refer to the standard deviation. Values for D, as measured from bulk and microfluidic experiments in this table, refer to the data in Figure 4, because D is dependent on the volume ratios (unlike pK', which, therefore, is a better standard for intersystem comparison).

DOI: 10.1021/acs.analchem.5b01061
Anal. Chem. 2015, 87, 6265–6270

■ ACKNOWLEDGMENTS

This work was partially funded by The Danish Council for Independent Research (grant number 09066477). Carl Esben Poulsen would like to thank The Oticon Foundation, The Otto Mønsted Foundation, and The Augustinus Foundation for funding.

■ REFERENCES

(1) *OECD Guidelines for the Testing of Chemicals: Partition Coefficient (n-octanol/water): Shake Flask Method*; Organisation for Economic Co-operation and Development: Paris, 1995.
(2) Alimuddin, M.; Grant, D.; Bulloch, D.; Lee, N.; Peacock, M.; Dahl, R. *J. Med. Chem.* **2008**, *51*, 5140−5142.
(3) Elvira, K. S.; Casadevall i Solvas, X.; Wootton, R. C. R.; deMello, A. J. *Nat. Chem.* **2013**, *5*, 905−915.
(4) Soares, R.; Novo, P.; Azevedo, A.; Fernandes, P.; Aires-Barros, M. R.; Chu, V.; Conde, J. P. *Lab Chip* **2014**, *14*, 4284−4294.
(5) Xiao, H.; Liang, D.; Liu, G.; Guo, M.; Xing, W.; Cheng, J. *Lab Chip* **2006**, *6*, 1067−1072.
(6) Marine, N. A.; Klein, S. A.; Posner, J. D. *Anal. Chem.* **2009**, *81*, 1471−1476.
(7) Mary, P.; Studer, V.; Tabeling, P. *Anal. Chem.* **2008**, *80*, 2680−2687.
(8) Miyaguchi, H.; Tokeshi, M.; Kikutani, Y.; Hibara, A.; Inoue, H.; Kitamori, T. *J. Chromatogr. A* **2006**, *1129*, 105−110.
(9) Kumemura, M.; Korenaga, T. *Anal. Chim. Acta* **2006**, *558*, 75−79.
(10) Chen, H.; Fang, Q.; Yin, X.-F.; Fang, Z.-L. *Lab Chip* **2005**, *5*, 719−725.
(11) Kralj, J. G.; Sahoo, H. R.; Jensen, K. F. *Lab Chip* **2007**, *7*, 256−263.
(12) Kralj, J. G.; Schmidt, M. A.; Jensen, K. F. *Lab Chip* **2005**, *5*, 531−535.
(13) Goyal, S.; Desai, A. V.; Lewis, R. W.; Ranganathan, D. R.; Li, H.; Zeng, D.; Reichert, D. E.; Kenis, P. J. *Sens. Actuators, B* **2014**, *190*, 634−644.
(14) Wagli, P.; Chang, Y.; Homsy, A.; Hvozdara, L.; Herzig, H. P.; de Rooij, N. F. *Anal. Chem.* **2013**, *85*, 7558−7565.
(15) Baret, J.-C. *Lab Chip* **2012**, *12*, 422−433.
(16) Kistrup, K.; Poulsen, C. E.; Østergaard, P. F.; Haugshøj, K. B.; Taboryski, R.; Wolff, A.; Hansen, M. F. J. *J. Micromech. Microeng.* **2014**, *24*, 125007.
(17) Andresen, K. Ø.; Hansen, M.; Matschuk, M.; Jepsen, S. T.; Sørensen, H. S.; Utko, P.; Selmeczi, D.; Hansen, T. S.; Larsen, N. B.; Rozlosnik, N.; Taboryski, R. J. *J. Micromech. Microeng.* **2010**, *20*, 055010.
(18) Yu, J.; Chin, L.; Chen, Y.; Zhang, G.; Lo, G. J. In *MicroTAS 2010*, Groningen, The Netherlands, Oct. 3−7, 2010; pp 1079−1081.
(19) Clarke, F. H. *J. Pharm. Sci.* **1984**, *73*, 226−230.
(20) Warhurst, D. C.; Craig, J. C.; Adagu, I. S.; Meyer, D. J.; Lee, S. Y. *Malar. J.* **2003**, *2*, 26.
(21) Schulman, S. G.; Threatte, R. M.; Capomacchia, A. C.; Paul, W. L. *J. Pharm. Sci.* **1974**, *63*, 876−880.

DOI: 10.1021/acs.analchem.5b01061
Anal. Chem. 2015, 87, 6265−6270